

CONDITION FOR CAPTURE INTO FIRST-ORDER MEAN MOTION RESONANCES AND APPLICATION TO CONSTRAINTS ON ORIGIN OF RESONANT SYSTEMS

MASAHIRO OGIHARA

Nagoya University, Furo-cho, Chikusa-ku, Nagoya, Aichi 464-8602, Japan

AND

HIROSHI KOBAYASHI

Nagoya University, Furo-cho, Chikusa-ku, Nagoya, Aichi 464-8602, Japan

Draft version June 26, 2021

ABSTRACT

We investigate the condition for capture into first-order mean motion resonances using numerical simulations with a wide range of various parameters. In particular, we focus on deriving the critical migration timescale for capture into the 2:1 resonance; additional numerical experiments for closely spaced resonances (e.g., 3:2) are also performed. We find that the critical migration timescale is determined by the planet-to-stellar mass ratio, and its dependence exhibits power-law behavior with index $-4/3$. This dependence is also supported by simple analytic arguments. We also find that the critical migration timescale for systems with equal-mass bodies is shorter than that in the restricted problem; for instance, for the 2:1 resonance between two equal-mass bodies, the critical timescale decreases by a factor of 10. In addition, using the obtained formula, the origin of observed systems that include first-order commensurabilities is constrained. Assuming that pairs of planets originally form well separated from each other and then undergo convergent migration and are captured in resonances, it is possible that a number of exoplanets experienced rapid orbital migration. For systems in closely spaced resonances, the differential migration timescale between the resonant pair can be constrained well; it is further suggested that several exoplanets underwent migration that can equal or even exceed the type I migration rate predicted by the linear theory. This implies that some of them may have formed *in situ*. Future observations and the use of our model will allow us to statistically determine the typical migration speed in a protoplanetary disk.

Subject headings: methods: numerical – celestial mechanics – planets and satellites: formation – planet-disk interactions

1. INTRODUCTION

When two bodies are in a mean motion resonance, their orbital periods are close to a ratio of two integers, which stabilizes the system in many cases. The Laplace 4:2:1 resonance among the Galilean satellites and the 3:2 resonances between Neptune and trans-Neptunian objects (TNOs) are well-known examples in the solar system.

More than 30 exoplanet systems also include confirmed planets exhibiting mean motion resonances. In addition, *Kepler* has detected a large number of planet pairs near mean motion resonances (e.g., Lissauer et al. 2011; Baruteau & Papaloizou 2013), although they are not necessarily in resonances. Many exoplanets are not near mean motion resonances (e.g., Mayor et al. 2009). However, according to Ogihara & Ida (2009), such non resonant configurations can be established through orbit crossing among the planets after they are captured in mutual mean motion resonances. Thus, mean motion resonances may have played an important role in the planet formation process.

To date, mean motion resonances have been studied from many perspectives (e.g., Goldreich 1965; Wisdom 1980; Henrard 1982; Weidenschilling & Davis 1985; Nelson & Papaloizou 2002; Kley et al. 2004; Terquem & Papaloizou 2007; Raymond et al. 2008;

Ogihara & Ida 2009; Ogihara et al. 2010). Resonant configurations are thought to arise primarily from convergent migration (e.g., Snellgrove et al. 2001). Several efforts have been made to derive a critical differential (relative) migration timescale $t_{a,\text{crit}}$ above which mean motion resonances can be formed.

Friedland (2001) analytically studied the restricted three-body problem with adiabatic migrating bodies, where the relative migration timescale is much longer than the resonant libration timescale. In contrast, recent studies have adopted numerical methods. One approach is to perform direct N -body calculations (e.g., Ida et al. 2000; Wyatt 2003), which take a direct summation of the mutual interaction between the bodies. Another approach uses the Hamiltonian model (e.g., Quillen 2006; Mustill & Wyatt 2011), where the canonical equations of the Hamiltonian are solved numerically with some approximations. These studies examine the dependence of the critical migration timescale on the mass but consider the restricted three-body problem with a massive planet and a massless test particle. Rein et al. (2010, 2012) performed direct N -body calculations with equal-mass planets. However, because their goal was to specify the origin of individual systems, the planetary mass was not usually treated as a parameter.

Our main aim is to derive an empirical formula for the critical migration timescale of capture into first-order $p + 1 : p$ mean motion resonances by performing direct

N -body simulations. We handle the physical variables (e.g., mass and damping timescales) as parameters and vary them over wide ranges. In this way, the dependences of the critical migration timescale on the parameters can be obtained. Although the equal-mass case is of primary importance for the study of observed exoplanets in resonances, previous general studies, which are not restricted to particular systems, have not considered this situation; therefore, we examine the case of equal-mass bodies. Captures into 2:1 resonances, which are the outermost first-order resonances, are extensively studied in this paper; in addition, more closely spaced commensurabilities (e.g., 3:2 and 4:3) are also examined. From the empirical formula based on our numerical results, we try to constrain the origin of the orbital architecture of planetary systems exhibiting commensurabilities.

The structure of this paper is as follows. In Section 2, we describe the numerical methods; in Section 3, we present and summarize the results of N -body simulations. In Section 4, we derive the mass dependence of the critical migration time, and in Section 5, we compare our results with those of previous studies. In Section 6, we apply these results to systems with resonances and discuss their origin, and in Section 7, we offer our conclusion.

2. NUMERICAL MODEL

Figure 1 presents the calculation model considered in this work. Initially, two planets with masses of M_1 (inner body) and M_2 (outer body) are placed at semimajor axes a_1 and a_2 , respectively. The initial eccentricity of these bodies is set to e_{ini} , and their inclination is also set to about e_{ini} in radian. Damping forces are applied to the bodies that damp the eccentricity and semimajor axis on timescales of t_e and t_a , respectively. We apply the a -damping force only to one body (mostly to the outer body); therefore, t_a is interpreted as the timescale of differential migration between the bodies. The initial locations are adopted to be separated from the resonance $a_2/a_1 = [(p+1)/p]^{2/3}$; namely, $a_2 = 1.8a_1$ for 2:1 resonance, and for other closer resonances (e.g., $p = 2$) the orbits are set just inside the $p : p - 1$ resonance $a_2/a_1 = [p/(p-1)]^{2/3}$. Thus, when t_e is much shorter than t_a , the eccentricity is negligibly small at the resonant encounter.

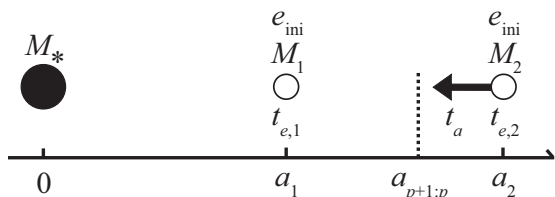


FIG. 1.— The model considered in this paper. Two bodies of masses M_1 and M_2 with orbits of semimajor axes a_1 and a_2 , respectively, around a central body with mass M_* . The initial eccentricities are set to e_{ini} . The orbits of the inner and outer bodies are circularized on timescales of $t_{e,1}$ and $t_{e,2}$, respectively. We assume the outer body undergoes inward migration on the timescale of t_a to see capture into a $p + 1 : p$ mean motion resonance.

The equation of motion for planet 2 is

$$\frac{d^2 \mathbf{r}_2}{dt^2} = -GM_* \frac{\mathbf{r}_2}{|\mathbf{r}_2|^3} - GM_1 \frac{\mathbf{r}_2 - \mathbf{r}_1}{|\mathbf{r}_2 - \mathbf{r}_1|^3}$$

TABLE 1
PARAMETERS

Parameters	Fiducial value	Parameter range
$M_1 (M_{\oplus})$	1	$10^{-1} - 10^3$
M_2/M_1	10^{-2}	$10^{-3} - 1$
$t_{e,1} (T_K)$	∞	$10^2 - \infty$
$t_{e,2} (T_K)$	10^3	$10^2 - \infty$
e_{ini}	10^{-4}	$10^{-4} - 10^{-1}$

NOTE. — Parameters and their ranges assumed. Parameters are described in Figure 1 and its caption.

$$-GM_1 \frac{\mathbf{r}_1}{|\mathbf{r}_1|^3} - GM_2 \frac{\mathbf{r}_2}{|\mathbf{r}_2|^3} + \mathbf{F}_e + \mathbf{F}_a, \quad (1)$$

where the first term on the right-hand side is the gravitational force of the central star, the second term is the mutual gravity between the bodies, and the third and fourth are the indirect terms. $\mathbf{F}_e = -2(\dot{\mathbf{r}}_2 \cdot \mathbf{r}_2)\mathbf{r}_2/|\mathbf{r}_2|^2 t_e$ and $\mathbf{F}_a = -\dot{\mathbf{r}}_2/t_a$ are the specific forces for e -damping and a -damping, respectively (see, for example, McNeil et al. 2005). The orbits are directly integrated with the fourth-order Hermite scheme (Makino & Aarseth 1992) over about 0.2 times the migration timescale, which means that although the long-term stability is not examined in this study, a temporary capture with a capture duration of less than about 0.1 times the migration timescale can be excluded.

In order to derive critical values of t_a for resonance capture, numerical simulations are performed with different t_a . The sampling interval of t_a adopted in this study is usually 0.2 in a logarithmic scale. We treat the masses (M_1 and M_2), the e -damping timescales ($t_{e,1}$ and $t_{e,2}$), and the initial eccentricity (e_{ini}) as parameters. For a fiducial model, the values are $M_1 = 1M_{\oplus}$, $M_2 = 10^{-2}M_{\oplus}$, $t_{e,1} = \infty$, $t_{e,2} = 10^3 T_K$, and $e_{\text{ini}} = 10^{-4}$, as shown in Table 1. Here, T_K indicates the orbital period of the inner body. We perform a series of calculations for a wide range of parameters to examine the dependences of resonant capture.

The equation of motion can be normalized by the unit length r_0 , unit mass M_* , and unit time $\Omega_K^{-1} = (GM_*/r_0^3)^{-1/2}$ as

$$\begin{aligned} \frac{d^2 \tilde{\mathbf{r}}_2}{dt^2} = & -\frac{\tilde{\mathbf{r}}_2}{|\tilde{\mathbf{r}}_2|^3} - \tilde{M}_1 \frac{\tilde{\mathbf{r}}_2 - \tilde{\mathbf{r}}_1}{|\tilde{\mathbf{r}}_2 - \tilde{\mathbf{r}}_1|^3} \\ & - \tilde{M}_1 \frac{\tilde{\mathbf{r}}_1}{|\tilde{\mathbf{r}}_1|^3} - \tilde{M}_2 \frac{\tilde{\mathbf{r}}_2}{|\tilde{\mathbf{r}}_2|^3} \\ & + \tilde{\mathbf{F}}_e + \tilde{\mathbf{F}}_a, \end{aligned} \quad (2)$$

where values with tildes on top are those scaled by the unit values. Therefore, by changing M_1 and M_2 , we can discuss the dependence on the stellar mass. Hereafter, we usually use $M_* = M_{\odot}$ and present M_1 and M_2 in units of Earth mass for simplicity. In this paper, we mostly present results assuming $M_1 \geq M_2$ because we find that the condition for capture into resonance is approximately expressed by the mass of the larger body, which will be shown in Section 3.8.

3. RESULTS

3.1. Procedure for Obtaining Critical Migration Timescale

We estimate the critical migration timescale in a manner similar to that of Wyatt (2003). Orbital integrations of two planets are performed with various parameters to determine whether the planets are captured into 2:1 mean motion resonances. Figure 2 shows the evolution of the semimajor axes and eccentricities of the two planets with a migration timescale t_a of $1.59 \times 10^7 T_K$ in the fiducial model. When a 2:1 commensurability is formed at $t \simeq 1.7 \times 10^6 T_K$, the eccentricities are excited. We also confirm that the two resonant angles¹ librate about fixed values.

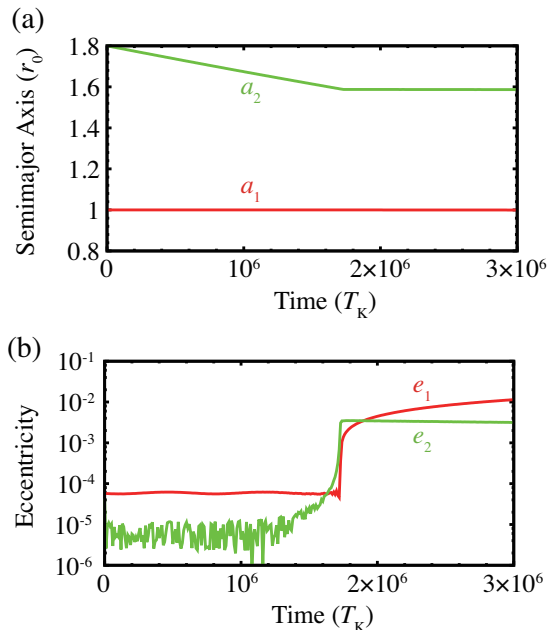


FIG. 2.— Example of orbital evolution, where the migration timescale of the outer body is assumed to be $1.59 \times 10^7 T_K$. (a) Evolution of semimajor axes. (b) Evolution of eccentricities. Two bodies are captured into the 2:1 mean motion resonance at $t \simeq 1.7 \times 10^6 T_K$.

We made 10 runs for each migration timescale with different initial orbital phase angles and derived the capture probability P of 2:1 resonances. When the period ratio lies within an error of 1%, we call it a resonant capture. Note that the long-term stability of the resonant configuration is not considered. Figure 3(a) shows the capture probability for the fiducial model as a function of the migration time. The probability P is assumed to have the form

$$P = \left[1 + \left(\frac{t_a}{t_{a,\text{crit}}} \right)^\gamma \right]^{-1}, \quad (3)$$

where $t_{a,\text{crit}}$ is defined as the migration time for which $P = 0.5$ and γ is a constant. Using a least-squares fit to the data (solid line), we specify $t_{a,\text{crit}}$ and γ . The capture probability increases sharply at $t_a \simeq 1.1 \times 10^7 T_K$, which

¹ The corresponding resonant angles are $\theta_1 = \lambda_1 - 2\lambda_2 + \varpi_1$ and $\theta_2 = \lambda_1 - 2\lambda_2 + \varpi_2$, where λ_i and ϖ_i are mean orbital longitudes and longitudes of the pericenter, respectively.

means that the critical migration time $t_{a,\text{crit}}$ can be estimated without introducing large errors ($\gamma \lesssim -300$). Figure 3(b) presents the results for an initial eccentricity of $e_{\text{ini}} = 0.01$. In this case, the eccentricity is 0.01 at the resonant encounter because the inner body does not undergo eccentricity damping. In contrast to low e_{ini} , high eccentricities reduce P at $t_a = 10^7 - 10^8 T_K$, and P gradually increases with t_a ($\gamma \simeq -2.2$). This broadening of the capture probability curve at higher eccentricity is also seen in previous studies (e.g., Quillen 2006; Mustill & Wyatt 2011). We find that the critical migration timescale can be sharply defined except when the eccentricity is not small ($e \gtrsim 0.01$) at the resonant encounter. In the following subsections, the value of γ is explicitly described only when the transition is not sharp enough. The eccentricity dependence of P is summarized in Section 3.5. We performed ~ 100 runs for each set of parameters ($\sim 15,000$ runs in total).

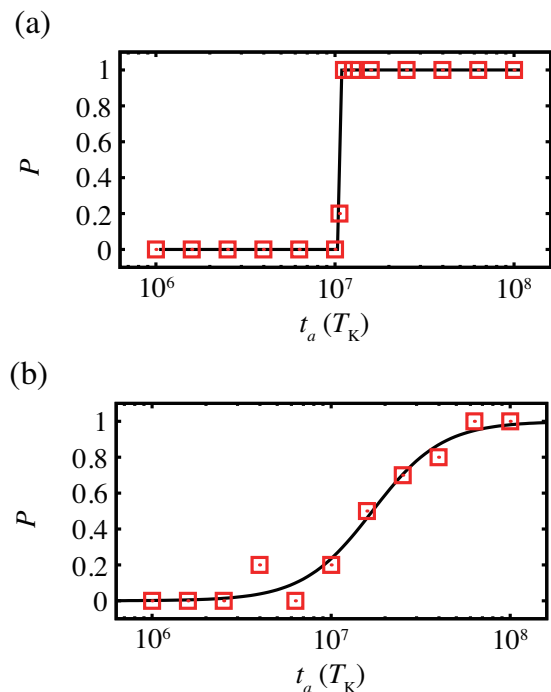


FIG. 3.— Capture probability versus migration timescale for (a) the fiducial model and (b) the model having relatively high initial eccentricities ($e_{\text{ini}} \simeq 0.01$). A least-squares fit to the data (solid lines) allows the critical migration timescale (t_a for $P = 0.5$) to be specified.

3.2. Dependence on M_1

We first examine the dependence of the critical migration timescale on the mass of the larger body M_1 . Figure 4 illustrates how $t_{a,\text{crit}}$ varies with M_1 . Open squares (connected by a solid line) represent the fiducial case, where $M_2/M_1 = 10^{-2}$, $t_{e,1}/T_K = \infty$, $t_{e,2}/T_K = 10^3$, and $e_{\text{ini}} = 10^{-4}$, with different values of M_1 . Filled squares, open circles, filled circles, and open triangles show the results for $M_1/M_2 = 1$, $t_{e,1}/T_K = 10^3$, $t_{e,2}/T_K = \infty$, and $e_{\text{ini}} = 10^{-2}$, respectively, but the other parameters are the same as for the fiducial case. Note that the open squares and open circles overlap at every M_1 . The dependence on M_1 is examined between $M_1/M_\oplus = 10^{-1}$

and 10^2 . In order to keep computational cost reasonable, we also put an upper limit of $t_{a,\text{crit}} = 10^8 T_K$. For $e_{\text{ini}} = 10^{-2}$, the eccentricity of the inner body is $\simeq 0.01$ at the resonant encounter and the capture probability curve is broadened ($\gamma \simeq -2$ – -4).

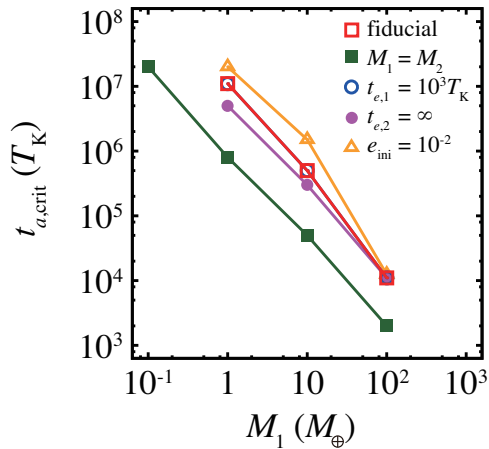


FIG. 4.— Critical migration timescale versus mass for larger body. Open squares represent the fiducial model. Filled squares, open circles, filled circles, and open triangles are the results for $M_1/M_2 = 1$, $t_{e,1}/T_K = 10^3$, $t_{e,2}/T_K = \infty$, and $e_{\text{ini}} = 10^{-2}$, respectively.

This survey reveals two features. First, all of the $t_{a,\text{crit}}$ values except that for $M_1/M_2 = 1$ are within about a factor of two of each other. This suggests that $t_{a,\text{crit}}$ depends weakly on $t_{e,1}$, $t_{e,2}$, and e_{ini} , which can be seen in the following subsections in more detail. Second, all the cases exhibit a similar power-law dependence of $t_{a,\text{crit}}$ on M_1 . The gradients are calculated for each case by least-squares fits, and we obtain a typical power index approximately equal to $-4/3$. A physical interpretation for this dependence is discussed in Section 4.

3.3. Dependence on M_2/M_1

Next, we explore the effect of varying M_2/M_1 . Note that the dependence can be seen more clearly when M_2/M_1 is used instead of M_2 . Figure 5 shows $t_{a,\text{crit}}$ as a function of M_2/M_1 . Open squares represent the fiducial case. Filled squares, open circles, filled circles, and open triangles show the results for $M_1/M_{\oplus} = 10^2$, $t_{e,1}/T_K = 10^3$, $t_{e,2}/T_K = \infty$, and $e_{\text{ini}} = 10^{-2}$, respectively. Same as the previous subsection, the capture probability curve is not sharp for $e_{\text{ini}} = 10^{-2}$ ($\gamma \simeq -1$ – -3).

We find that if $M_2/M_1 \lesssim 10^{-1}$, $t_{a,\text{crit}}$ is independent of M_2/M_1 ; therefore, the restricted three-body approximation is valid for this condition. The difference between $t_{a,\text{crit}}$ for $M_2/M_1 = 1$ and the value for small M_2/M_1 is found to be a factor of about 10. Thus, although the restricted three-body approach cannot provide an accurate prediction of $t_{a,\text{crit}}$ for bodies with comparable masses, it would be possible to roughly derive $t_{a,\text{crit}}$ to an accuracy of a factor of 10. See also discussions in Sections 3.8 and 5 for the reason for the difference.

Note that we consider only the migration of the outer planet. Because migration speed depends on planetary mass, the inner planet’s migration is not negligible, especially for $M_1 \sim M_2$. However, if we apply the differential

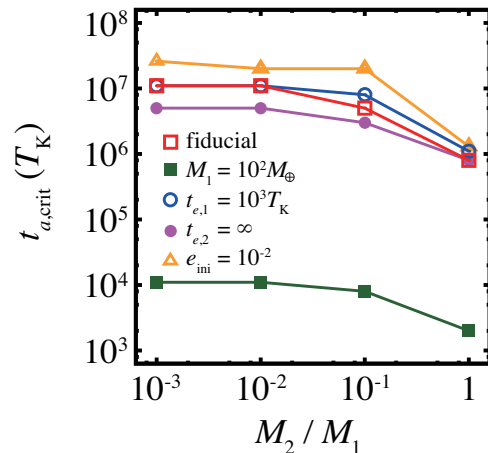


FIG. 5.— Critical migration timescale versus M_2/M_1 . Open squares represent the fiducial model. Filled squares, open circles, filled circles, and open triangles represent the results for $M_1/M_{\oplus} = 10^2$, $t_{e,1}/T_K = 10^3$, $t_{e,2}/T_K = \infty$ and $e_{\text{ini}} = 10^{-2}$, respectively.

migration speed instead of the migration speed of the outer planet, the critical migration timescales we obtain are valid even considering the migration of both planets.

3.4. Dependence on t_e

Figure 6 shows the results for various eccentricity-damping timescales for the inner (larger) planet, $t_{e,1}$. Again, the open squares represent the fiducial case. Filled squares, open circles, filled circles, and open triangles show the results for $M_1/M_{\oplus} = 10^2$, $M_1/M_2 = 1$, $t_{e,2}/T_K = \infty$, and $e_{\text{ini}} = 10^{-2}$, respectively. The rightmost points on the horizontal axis are the cases without eccentricity damping. For $e_{\text{ini}} = 10^{-2}$ and $t_{e,1} = \infty$, the transition from a capture probability of zero to one is not very sharp ($\gamma \simeq -2$). There is no systematic change in $t_{a,\text{crit}}$ with $t_{e,1}$. Even when $t_{e,1}$ is varied by more than four orders of magnitude, the differences in $t_{a,\text{crit}}$ lie within a factor of two or three.

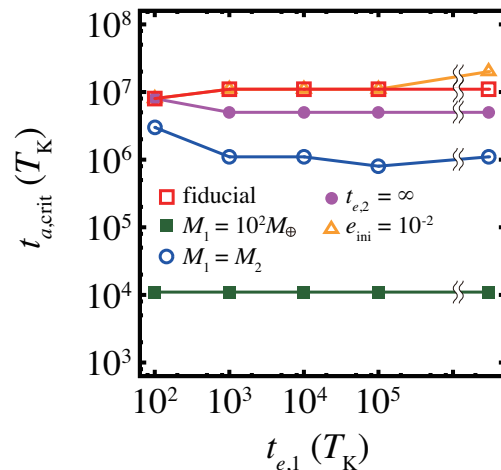


FIG. 6.— Critical migration timescale versus $t_{e,1}$. Open squares are the fiducial case. Filled squares, open circles, filled circles, and open triangles represent the results for $M_1/M_{\oplus} = 10^2$, $M_1/M_2 = 1$, $t_{e,2}/T_K = \infty$, and $e_{\text{ini}} = 10^{-2}$, respectively.

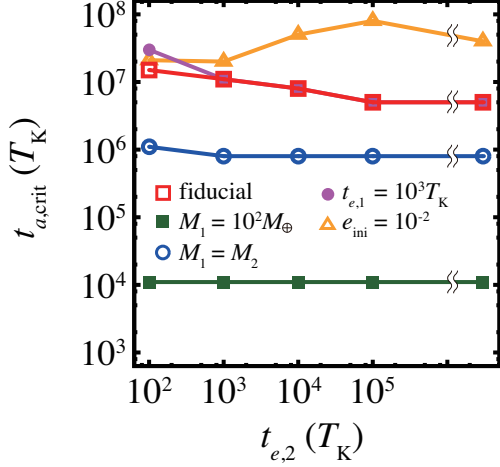


FIG. 7.— Critical migration timescale versus $t_{e,2}$. Open squares represent the fiducial case. Filled squares, open circles, filled circles, and open triangles represent the results for $M_1/M_\oplus = 10^2$, $M_1/M_2 = 1$, $t_{e,1}/T_K = 10^3$, and $e_{\text{ini}} = 10^{-2}$, respectively.

Figure 7 shows the results for various eccentricity–damping timescales for the outer (smaller) planet, $t_{e,2}$. Open squares represent the fiducial case. Filled squares, open circles, filled circles, and open triangles are the results for $M_1/M_\oplus = 10^2$, $M_1/M_2 = 1$, $t_{e,1}/T_K = 10^3$, and $e_{\text{ini}} = 10^{-2}$, respectively. For $e_{\text{ini}} = 10^{-2}$, the transition in the capture probability is not sharp ($\gamma \simeq -2$ – -6). We also do not see any clear trends in $t_{e,2}$. Although the case with $e = 10^{-2}$ (open triangles) shows a slight variation, it still remains within a factor of a few.

3.5. Dependence on e_{ini}

Finally, Figure 8 shows the results for various initial eccentricities e_{ini} . Open squares represent the fiducial case. Filled squares, open circles, filled circles, and open triangles are the results for $M_1/M_\oplus = 10^2$, $M_1/M_2 = 1$, $t_{e,1}/T_K = 10^3$, and $t_{e,2}/T_K = \infty$, respectively. When the eccentricity is not small ($e \gtrsim 0.01$) at the resonant encounter, in other words, when $e_{\text{ini}} \geq 10^{-2}$ and $t_e > t_a$, the capture probability curve is not sharp the same as before. Again, no clear trends in $t_{a,\text{crit}}$ with e_{ini} are recognized. Note that, for $e_{\text{ini}} = 10^{-1}$ and $M_1/M_2 = 1$ (open circles) and for $t_{e,2}/T_K = \infty$ (open triangles), $t_{a,\text{crit}}$ cannot be determined to have particular values. Because the eccentricity of the smaller body M_2 at a resonant encounter is relatively large, adequate resonant capture does not occur even for long t_a ; the capture probability does not exceed about 0.3. Except for large e_{ini} , the dependence is reasonably weak. Several of these features are in agreement with previous studies, which will be discussed in Section 5.

3.6. Summary of Results

The critical migration timescales derived in the previous subsections are summarized as follows:

$$t_{a,\text{crit}} \simeq \begin{cases} 1 \times 10^7 \left(\frac{M_1}{M_\oplus}\right)^{-4/3} \left(\frac{M_*}{M_\odot}\right)^{4/3} T_K & (M_2/M_1 \lesssim 0.1) \\ 1 \times 10^6 \left(\frac{M_1}{M_\oplus}\right)^{-4/3} \left(\frac{M_*}{M_\odot}\right)^{4/3} T_K & (M_2/M_1 \simeq 1), \end{cases} \quad (4)$$

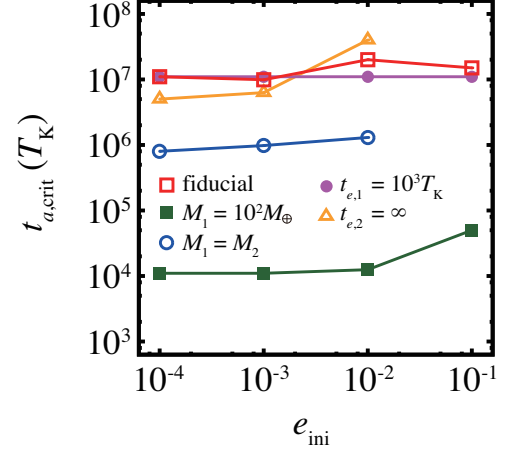


FIG. 8.— Critical migration timescale versus initial eccentricity. Open squares represent the fiducial case. Filled squares, open circles, filled circles, and open triangles represent the results for $M_1/M_\oplus = 10^2$, $M_1/M_2 = 1$, $t_{e,1}/T_K = 10^3$ and $t_{e,2}/T_K = \infty$, respectively.

where the dependence on the stellar mass M_* is included. As shown in the results, $t_{a,\text{crit}}$ can differ by a factor of two or three. Although we assume that the inner body is more massive than the outer body ($M_1 \geq M_2$), the results are almost the same when the outer one is more massive, which will be seen in Section 3.8. The formula is valid if the eccentricities of the smaller planets at a resonant encounter are much smaller than 0.1.

3.7. Closely Spaced Resonances

The capture condition for 2:1 mean motion resonances was examined above. We performed additional simulations to evaluate the critical migration timescale for closely spaced first–order resonances (e.g., 3:2 and 4:3) because several exoplanet systems have such commensurabilities.

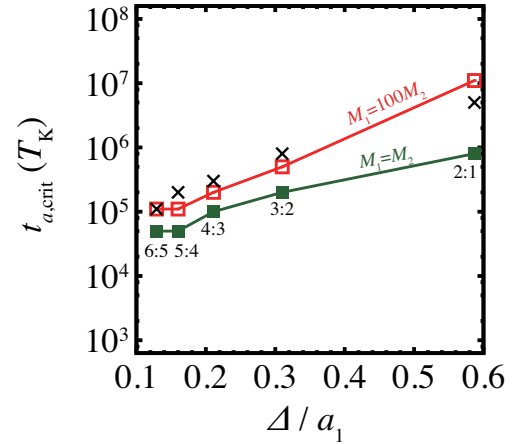


FIG. 9.— Critical migration timescales for 2:1 and more closely spaced resonances. Open and filled squares represent the results for $M_2/M_1 = 10^{-2}$ and $M_2/M_1 = 1$, respectively. Crosses represent the results for internal resonances ($M_1/M_\oplus = 10^{-2}$ and $M_2/M_\oplus = 1$).

Figure 9 shows the critical migration timescales for $p+1 : p$ resonances ($p = 1, 2, 3, 4, 5$) obtained by numerical

simulations. Here, we define

$$\Delta \equiv \left[\left(\frac{p+1}{p} \right)^{2/3} - 1 \right] a_1, \quad (5)$$

which roughly corresponds to the orbital separation from the inner planet to the outer planet in the mean motion resonance. Open squares represent the results for $M_2/M_1 = 10^{-2}$, whereas filled squares represent those for equal-mass bodies ($M_2/M_1 = 1$). In each case, the other parameters are set to the fiducial values ($M_1/M_\oplus = 1$, $t_{e,1}/T_K = \infty$, $t_{e,2}/T_K = 10^3$, $e_{\text{ini}} = 10^{-4}$). We see that the critical migration time decreases with decreasing separation. The critical migration timescale for equal-mass bodies ($M_1 = M_2$) is always shorter than that with bodies that have a high mass ratio ($M_1 = 100M_2$). The difference in $t_{a,\text{crit}}$ is larger at 2:1 resonances than at closely spaced resonances. This is presumably because the strength of the 2:1 external resonance, where “external” means that the inner body is the dominant body, is significantly weakened by indirect terms in the disturbing function, which will also be discussed in Section 3.8.

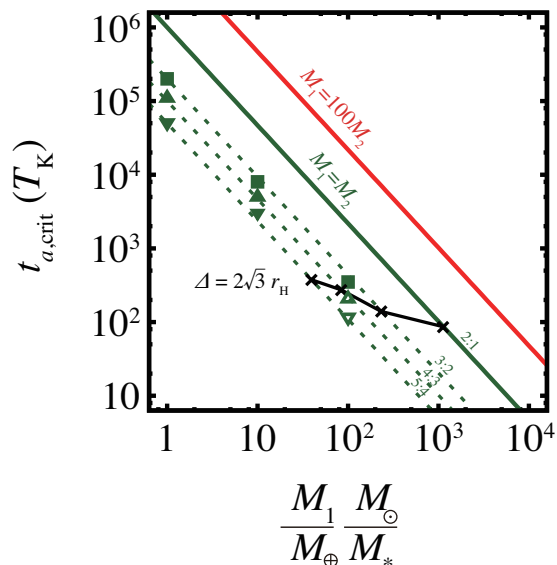


FIG. 10.— Summary of critical migration timescale derived from numerical simulations. Solid and dashed lines represent the critical migration timescales for 2:1 and more closely spaced resonances, respectively. Filled symbols indicate the numerically determined values, whereas for open symbols, $t_{a,\text{crit}}$ cannot be derived owing to close encounters. The orbital separation Δ divided by the mutual Hill radius r_H can be expressed in terms of the mass and semimajor axis. The masses of $\Delta = 2\sqrt{3} r_H$ for each resonance are plotted with crosses and connected by a solid line by assuming $M_1 = M_2$.

The combined results from the above surveys are plotted in Figure 10. The solid lines indicate the critical migration timescale for capture into the 2:1 resonance as a function of M_1 , which is summarized in Equation (4). Squares, triangles, and inverted triangles are the numerical results for the 3:2, 4:3, and 5:4 resonances, respectively. From the results, the critical migration timescale is described as

$$t_{a,\text{crit}} = C \left(\frac{M_1}{M_\oplus} \right)^{-4/3} \left(\frac{M_*}{M_\odot} \right)^{4/3} T_K, \quad (6)$$

TABLE 2
FITTING RESULTS FOR C

Mass ratio	2:1	3:2	4:3	5:4	6:5
$M_2/M_1 \simeq 1$	1×10^6	2×10^5	1×10^5	5×10^4	5×10^4
$M_2/M_1 \lesssim 0.1$	1×10^7	5×10^5	2×10^5	1×10^5	1×10^5

NOTE. — Fitting results to Equation (6) for each mean motion resonance. Note that, for $M_2/M_1 \lesssim 0.1$ and the 3:2, 4:3, 5:4 and 6:5 resonances, the mass dependence is not examined, but the critical migration timescales are derived only for $M_1 = 1M_\oplus$ and $M_2 = 10^{-2}M_\oplus$.

where C depends on M_1/M_2 and the resonant commensurability. We derive the C values from the fitting of the results and summarize C in Table 2. Note that although C should depend on commensurability, the values are the same between the 5:4 and 6:5 resonances, which suggests that the difference is within the minimum interval of t_a that we set for our investigation. The dashed lines in Figure 10 represent fitting results for equal-mass cases ($M_1 = M_2$). Although the approximate fits for closer resonances are considered to be correct within a factor of a few, they should be treated with some caution. We observe that when $M_1/M_\oplus = 100$ and $p = 3, 4$, the bodies undergo close encounters before being captured into resonances; therefore, the bodies do not settle into stable resonant orbits, as indicated by the open symbols in Figure 10.

According to the analysis of the Hill stability by Gladman (1993), dynamical stability is almost guaranteed if $\Delta \gtrsim 2\sqrt{3} r_H$, where r_H is the mutual Hill radius. Note that if the orbital separation is within a few tens of percent beyond the critical Hill separation, Hill-stable planetary systems may manifest Lagrange instability when the outer planet escapes to infinity (Barnes & Greenberg 2005; Veras & Mustill 2013). There is no analytical criteria that describe Lagrange stability, and additional numerical simulation is required to determine whether the system is Lagrange stable or not. However, Barnes & Greenberg (2005) found that the Hill stable condition is a good predictor of Lagrange stability. The Hill stable condition is rewritten as

$$M_1 + M_2 \leq \frac{1}{\sqrt{3}} \left[\frac{(p+1)^{2/3} - p^{2/3}}{(p+1)^{2/3} + p^{2/3}} \right]^3 M_*. \quad (7)$$

The critical masses for equal-mass bodies assuming $M_* = M_\odot$ are plotted with crosses connected with by a solid line in Figure 10. If the mass of the body is larger than the critical mass, the system becomes Hill unstable, which is consistent with our results that exhibit close encounters (open symbols). Note that even if $\Delta \lesssim 2\sqrt{3}r_H$, the orbit in a resonance can become stable for specific orbital arguments (some examples are provided in Section 6). This criterion for the instability is a rough estimate, and long-term orbital integration can reveal the instability time of planets in closely spaced mean motion resonances.

3.8. Internal Resonances

So far, we have carried out simulations in the cases where the inner body is more massive or equal to the outer body. In order to evaluate the difference in $t_{a,\text{crit}}$ between the internal and external resonances, additional

simulations for outer massive body are performed. Assuming $M_1 = 10^{-2}M_\oplus$, $M_2 = 1M_\oplus$, $t_{e,1} = 10^3T_K$, $t_{e,2} = \infty$, and $e_{\text{ini}} = 10^{-4}$, the critical migration timescales are determined for 2:1, 3:2, 4:3, 5:4, and 6:5 resonances, which are plotted in Figure 9 with crosses.

We find that no significant difference between the internal and external resonances; in fact, it lies within a factor of two. Therefore, as stated in the last sentence of Section 2, if the outer body is larger than the inner body, we apply the mass of the larger body to M_1 ; Equation (6) is then valid.

Although the difference is not significant, we see a decrease in $t_{a,\text{crit}}$ at the 2:1 internal resonance, which means that the 2:1 internal resonance is stronger than the 2:1 external resonance. This tendency can be understood in terms of contributions of each term in the disturbing function. For the 2:1 external resonance, the contribution of the direct term is diminished by the indirect term, leading to weakening the strength of the resonance (Quillen 2006; Mustill & Wyatt 2011). One indicator of the strength of the resonance is l_j in the work of Mustill & Wyatt (2011) (see Table 1 in their work for each value), where the strength of resonance decreases with increasing l_j . We see that l_j for the 2:1 external resonance is large. The fact that the 2:1 internal resonance is stronger than the 2:1 external resonance would also partially explain the decrease in $t_{a,\text{crit}}$ for equal-mass bodies in Figures 5 and 9 although this cannot account for the entire change. We also see in Figure 9 that internal resonances are slightly weaker than external resonances for closely spaced resonances (e.g., 3:2), which is consistent with Figure 11 in the work of Mustill & Wyatt (2011).

4. ANALYSIS OF THE DEPENDENCE OF $T_{A,\text{CRIT}}$ ON M_1

We discuss the numerical results using analytical arguments. Through numerical investigations, we find that the critical migration timescale shows a power-law behavior, $t_{a,\text{crit}} \propto (M_1/M_*)^{-4/3}$, which was also seen in previous studies (e.g., Ida et al. 2000; Quillen 2006). This tendency can be estimated using a simple pendulum model (Murray & Dermott 1999); the following expressions describe the orbital properties of a massless particle that is in a mean motion resonance. Note that these expressions are for the internal resonance; however, those for the external resonance are almost the same. For the circular restricted problem, where the massless test particle is in a first-order $p+1 : p$ resonance with a body with mass of M , the maximum width of libration is given by

$$\Delta_{\text{res}} = \left[\frac{-16C_r e_{\text{res}}}{3n} \right]^{1/2} a, \quad (8)$$

where e_{res} is the excited eccentricity due to resonant perturbation, and n and a are the mean motion and semimajor axis of the test particle, respectively. The constant arising from the resonant term of the disturbing function is

$$C_r = -\frac{M}{M_*} n \alpha \left(p + 1 + \frac{\alpha}{2} D \right) b_{1/2}^{p+1}, \quad (9)$$

$$= \frac{M}{M_*} n \alpha f_d(\alpha), \quad (10)$$

where α , $b_{1/2}^{p+1}$, and D are the ratio of semimajor axis of the inner body to that of the outer body, the Laplace coefficient, and the derivative operator, respectively. For the first-order resonance, C_r is always negative. The libration timescale is derived as

$$\tau_{\text{lib}} = \frac{2\pi}{(-3p^2 C_r n e_{\text{res}})^{1/2}}. \quad (11)$$

Then the excited eccentricity during the resonant passage is approximated using an adiabatic invariant as

$$e_{\text{res}}^2 = \frac{\Delta_{\text{res}}}{pa}, \quad (12)$$

as in Zhou & Lin 2007. Substituting this equation into Equations (8) and (11), we obtain

$$e_{\text{res}} = \left(\frac{-16C_r}{3p^2 n} \right)^{1/3}, \quad (13)$$

$$\Delta_{\text{res}} = \left(\frac{-16C_r}{3n} \right)^{2/3} \frac{a}{p^{1/3}}, \quad (14)$$

$$\tau_{\text{lib}} = \left(\frac{n^2}{12p^2 C_r^2} \right)^{1/3} T_K. \quad (15)$$

Comparing the libration timescale τ_{lib} and the migration timescale through the resonant width τ_a , where

$$\tau_a = \frac{\Delta_{\text{res}}}{\dot{a}} = \frac{\Delta_{\text{res}} t_a}{a}, \quad (16)$$

we determine that the critical migration timescale can be roughly given by

$$t_{a,\text{crit}} = \left(\frac{-3}{1024p\alpha^4 f_d(\alpha)^4} \right)^{1/3} \left(\frac{M}{M_*} \right)^{-4/3} T_K. \quad (17)$$

We confirm the power-law dependence on the mass. In addition, given that $p = 1$, $\alpha = 0.63$, and $\alpha f_d(\alpha) \simeq -0.75$ (Murray & Dermott 1999), $t_{a,\text{crit}}$ for an Earth-mass body is $\sim 10^7 T_K$. These estimates are roughly consistent with our numerical results; note, however, that they are only order-of-magnitude estimates assuming the restricted problem. The contribution from the variation in the longitude of the pericenter ϖ is also neglected.

5. COMPARISON WITH PREVIOUS STUDIES

We here discuss our results by comparing with previous studies. First, our results for two bodies that have a high mass ratio can be compared to the works that consider the restricted problem (e.g., Quillen 2006; Mustill & Wyatt 2011). We find that several features in Figure 8, in which the dependence of $t_{a,\text{crit}}$ on the eccentricity is investigated, are in agreement with the results of Mustill & Wyatt (2011) (Figure 2 in their paper) as follows. Mustill & Wyatt (2011) showed that when the generalized momentum is small enough, which corresponds to small e , the capture probability curve is steep and $t_{a,\text{crit}}$ hardly depends on e . In Figure 8, we observe that $t_{a,\text{crit}}$ is well-defined and almost independent of e

when e at the resonant encounter is small ($e \lesssim 10^{-3}$ for $M_1 = 1M_\oplus$). In this case, the value of $t_{a,\text{crit}}$ is also comparable to that derived by Mustill & Wyatt (2011); that is, their estimate for $t_{a,\text{crit}}$ is $\simeq 4 \times 10^6 T_K$ for $M_1 = 1M_\oplus$. We also see another feature of steepening dependence on e at higher e . According to Mustill & Wyatt (2011), $t_{a,\text{crit}}$ tends to sensitively depend on e when e is larger than ~ 0.01 and ~ 0.05 for $M_1 = 1M_\oplus$ and $100M_\oplus$, respectively, which are seen in Figure 8 in the models of $t_{e,2} = \infty$ and $M_1 = 10^2 M_\oplus$. The other feature is that the capture probability has a cutoff at high eccentricity and never exceeds about 0.3 in the case of $t_{e,2} = \infty$. In our results, the cutoff eccentricity is $e \simeq 0.01$, which quantitatively reproduces the results of Mustill & Wyatt (2011).

In addition, several similar features are observed even in the results for equal-mass bodies; namely, the weak dependence of $t_{a,\text{crit}}$ on e and the existence of the cutoff in the capture probability at high e , which were expected from the previous study (Mustill & Wyatt 2011). Note, however, that the values of $t_{a,\text{crit}}$ differ by a factor of 10 between the restricted problem and the unrestricted problem. Even if we consider the difference between the internal resonance and the unrestricted problem, there is at least a factor of a few difference in $t_{a,\text{crit}}$. Special care would have to be taken when one quantitatively discuss the critical migration timescale for equal-mass bodies.

Several properties observed in our simulations were also seen in a dynamical study by Rein et al. (2012). Figure 2 of Rein et al. (2012) indicates the excluded resonant regions for the HD 200964 system; Figure 2(a) shows their results for two planets of comparable mass, whereas Figure 2(c) shows the case where one body is a test particle. They found that the allowed region for the comparable-mass case is wider than that for the zero-mass particle, which suggests that planets with comparable masses are more easily captured into mean motion resonances. In our model, we find that the critical migration timescale for equal-mass planets is shorter than that for systems with high mass ratios. In addition, we also see a weak dependence of the critical migration timescale on the e -damping timescales. This tendency is also seen in Figure 4 of Rein et al. (2012).

Papaloizou & Szuszkiewicz (2005) derived an analytical expression for the eccentricity of the outer planet captured into a resonance. The equilibrium eccentricity is attained by balancing pumping due to resonant effects with damping caused by migration, as described by Equation (5) of Papaloizou & Szuszkiewicz (2005). We confirmed that our numerical results are consistent with this analytical formula except for rapid migration ($t_e/t_a \gtrsim 0.1$) and equal-mass bodies.

6. CONSTRAINTS ON FORMATION MODELS

The results given in Section 3 can be used to constrain the history of systems in mean motion resonances and their formation scenarios. In this section, we first discuss exoplanet systems with resonances using the mass versus critical migration timescale diagram, and then move on to other systems.

6.1. Exoplanet Systems

As of 2013, more than 25 planetary systems that lie in or close to first-order mean motion resonances have

been detected (e.g., Steffen et al. 2013). Table 3 lists the orbital properties of the confirmed planets that could be in first-order resonances². The fourth and fifth columns show the masses and semimajor axes of the planets, respectively; the sixth and seventh columns show the resonant properties. For example, the third row indicates that Gliese 876 c could be in a 2:1 resonance with planet b, where the period ratio of these planets is 2.03. The data are taken from the Open Exoplanet Catalogue³. Note that many systems listed have ratios more distant from commensurability than the 1% used to classify resonant captures in our simulations. Although the period ratios are close to commensurate values, not all of the planets necessarily lie in mean motion resonances.

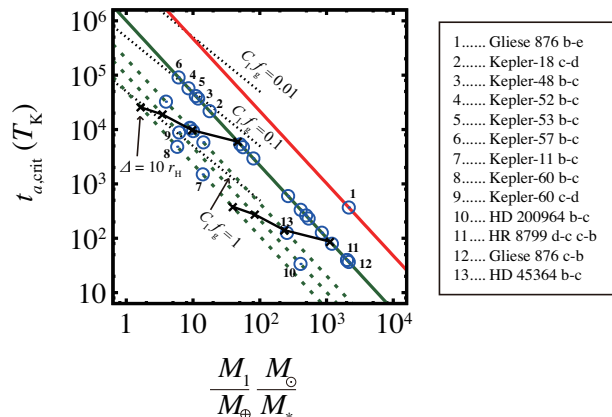


FIG. 11.— Same as Figure 10, but observed resonant pairs listed in Table 3 are also plotted as open circles, which indicate the critical migration timescale for each pair. This means that the pair would be moved in the gas disk on a relative migration timescale longer than the critical value. In addition to $\Delta = 2\sqrt{3}r_H$, $\Delta = 10r_H$ is also marked by crosses connected by a solid line, which indicate the typical orbital separation of planets formed via oligarchic growth. The three dotted lines represent the type I migration timescale with different migration efficiencies, $C_1 f_g = 1, 0.1$, and 0.01 .

The solid and dashed lines in Figure 11, which indicate the critical migration speeds, are the same as in Figure 10. For the resonant-pair exoplanets listed in Table 3, the critical migration timescale, plotted as open circles, is obtained from their resonant commensurability and the mass ratio between the smaller and larger bodies ($M_2/M_1 < 0.1$ or not) as a function of the larger planet mass. All pairs except for the pair of Gliese 876 b and e have roughly equal masses $M_2/M_1 > 0.1$. The outer planet migration timescale must be longer than the critical migration time for capture into mean motion resonance to occur. We obtained the critical migration timescale in Section 3 while ignoring the migration of inner planets. If the inner planets also migrate inward, the differential (or relative) migration speed between the inner and outer planets should be applied to the critical migration speed.

Using Figure 11, we can place some constraints on the differential migration speeds that the exoplanets used to have. Note that in the following discussions, we intro-

² This is taken from two papers (Szuszkiewicz & Podlowska-Gaca 2012; Steffen et al. 2013) and should not be a complete list.

³ <http://exoplanet.hanno-rein.de/>

duce several assumptions: (i) Planets formed widely separated from the 2:1 resonance. (ii) The masses of planets do not evolve after the onset of migration. (iii) Migration is smooth and not subjected to stochastic torques⁴. (iv) The eccentricities of planets are low and hence the transition from certain capture to certain failure is well-defined. (v) Once captured in resonance, planets do not subsequently escape from the resonance.

The 2:1 mean motion resonance is the outermost first-order mean motion resonance. The capture probability for the outer, higher-order mean motion resonance is very low. Therefore, if a system has a 2:1 commensurability, the differential migration speed would have been slower than that estimated from the critical migration time. If a system has a 3:2 commensurability, the outer planet passed through the 2:1 mean motion resonance because of the high migration speed and was captured into the 3:2 mean motion resonance; thus, the differential migration speeds is slower than the critical migration speed for the 3:2 mean motion resonance but faster than that for the 2:1 mean motion resonance. We can constrain the differential migration speed for capture in the other mean motion resonances in a similar manner. The pairs of exoplanets in the closely spaced mean motion resonances are expected to have migrated at significantly high speed.

Note that if two planets in a mean motion resonance formed with a small orbital separation, they may have been captured into closely spaced resonances under slow migration. In addition, if several planets simultaneously exhibit migration as a resonant convoy (McNeil et al. 2005; Ogihara & Ida 2009) rather than the single outer planet migrating inward, the critical migration timescale can be somewhat longer than that derived in Section 3. Nonetheless, our approach provides useful constraints on formation models without the need for further dynamical analyses and calculations for individual systems.

6.1.1. Overall Trend

Although the number of observed resonant exoplanets is too small to support a statistical discussion, we see in Figure 11 that there is a general trend toward a decrease in the number of systems in closely spaced resonances with increasing mass. This trend can be understood in terms of the short critical migration timescale for capture into 2:1 resonances with high-mass planets; 1000-Earth-mass planets can capture bodies into 2:1 resonances even if the migration timescale is quite short ($\simeq 100T_K$).

As stated in Section 3.7, it is predicted that pairs with orbital separations smaller than $\simeq 2\sqrt{3}$ Hill radii can be Hill unstable, and such configurations are rare. We note that the Hill stability criterion, more properly bodies should be Lagrange stable, gives only a sufficient condition for stability; thus, if the planets are in mean motion resonances, the system can become stable. However, they should experience a configuration where planets are not near resonances at some point during migration phase; therefore, it is possible that such planets undergo close encounters and are scattered away from

⁴ Rein (2012) have shown that orbital integrations that include some degree of stochasticity is necessary to reproduce the orbital period ratio distribution of the *Kepler* planet candidates. We assume smooth migration in this paper for simplicity.

the system. We find that almost all the pairs have separations larger than $\simeq 2\sqrt{3}r_H$; however, there are several exceptions. We discuss these systems in Section 6.1.3.

On the other hand, several pairs have separations larger than $\simeq 10$ Hill radii, which is the typical orbital separation of planets formed via the oligarchic growth phase (Kokubo & Ida 1998). The location of $\Delta = 10r_H$ is also shown in Figure 11 by crosses connected by a solid line, in the same way as for $\Delta = 2\sqrt{3}r_H$. Thus, planets are believed to form in distant orbits, after which they migrate inward one by one, maintaining their orbital separations wider than $10r_H$ (Ogihara & Ida 2009). These systems include Kepler-18, Kepler-48, Kepler-52, Kepler-53, and Kepler-57, which all have 2:1 commensurabilities. Figure 11 gives the lower limits on the migration timescale.

For example, the Kepler-18 system consists of two low-density Neptune-mass planets (c and d) near a 2:1 resonance and an inner super-Earth (b) (Cochran et al. 2011). The orbital separation of planets c and d is $\simeq 13r_H$. The planets are believed to undergo migration with a differential migration speed slower than $2 \times 10^4 T_K$.

Next, we focus on super-Earth-mass planets ($M \sim 10M_\oplus$), which have a relatively large number of samples, and compare their histories with the migration theory. Planets with a few tens of the Earth mass or less might have experienced type I migration. Through a linear calculation, the type I migration timescale is given by (Tanaka et al. 2002)

$$t_{a,\text{lin}} = \frac{1}{2.7 + 1.1q} \left(\frac{M}{M_*}\right)^{-1} \left(\frac{\Sigma_g r^2}{M_*}\right)^{-1} \left(\frac{c_s}{v_K}\right)^2 \Omega_K \quad (18)$$

where $-q$ denotes the surface density gradient. For optically thin disks, the temperature distribution is (Hayashi 1981)

$$T \simeq 280 \left(\frac{r}{1\text{AU}}\right)^{-1/2} \left(\frac{L_*}{L_\odot}\right)^{1/4} \text{K}, \quad (19)$$

which determines the sound velocity c_s . We scale the gas surface density as

$$\Sigma_g = 2400 f_g \left(\frac{r}{1\text{AU}}\right)^{-q} \text{g cm}^{-2}, \quad (20)$$

where f_g is a scaling factor. If we introduce the type I migration efficiency $C_I \equiv t_{a,\text{lin}}/t_a$ to express the uncertainty in the type I migration theory, the type I migration timescale for $q = 3/2$ and $L_* = L_\odot$ is written as

$$t_a = 5.0 \times 10^4 C_I^{-1} f_g^{-1} \left(\frac{M}{M_\oplus}\right)^{-1} T_K. \quad (21)$$

The type I migration speed is still uncertain⁵. Here, we consider a scenario in which the inner body is stationary and the outer body undergoes inward migration. Then the type I migration timescale (Equation [21]), which is identical to the relative migration timescale between the two bodies, can be drawn as a function of $C_I f_g$ (dotted line in Figure 11).

⁵ In an optically thick disk, the migration timescale can be long, and outward migration is possible under some conditions (Paardekooper et al. 2011). A population synthesis model by Ida & Lin (2008) suggests that the typical migration efficiency is less than that obtained by linear analysis ($C_I \lesssim 0.1$).

Some of the exoplanets with masses of $\sim 10M_{\oplus}$ are in 2:1 resonances. As shown in Figure 11, they would not have undergone rapid migration, so $C_{1f_g} \lesssim 0.1$. On the other hand, some planets are captured into closely spaced resonances. For them, a short migration time is required, and $C_{1f_g} \sim 1$.

In order to reconcile the low migration efficiency ($C_{1f_g} \lesssim 0.1$) and the linear type I migration theory, the migration of inner planets should be considered. If the inner planets migrate when they are captured into mean motion resonances, the differential migration speeds become much slower than the migration rate estimated from Equation (18). This can explain the planets in the 2:1 mean motion resonances. On the other hand, the migration of inner planets is negligible if the inner planets are much smaller than the outer ones and/or if the inner planets have orbits around the inner edge of the disk. Such pairs of planets can be in closely spaced resonance because of the high relative migration speed.

In addition, the other possibility for a pileup of planets with masses of $\simeq 10M_{\oplus}$ is that they are formed near the current resonance locations (e.g., 3:2 and 2:1). The orbital separations for 10–Earth–mass planets in 3:2 and 2:1 resonances are $\simeq 10r_H$ and $\simeq 15r_H$, respectively. This is comparable to the typical separation after the oligarchic growth phase: planets are formed *in situ* and then migrate slightly and are captured in the resonances.

As argued above, the formation of resonances between two planets can be discussed in terms of two cases of the orbital separation at the time migration begins; namely, the planets are well separated from each other ($\Delta > 10r_H$), or they have relatively close orbits ($\Delta \simeq 10r_H$). The orbital separation of the planets at the onset of migration is characterized by their migration and growth timescales. The growth timescale of a planet t_g is determined by the accretion rate of surrounding planetesimals in the classical planet growth model, which is similar to or longer than the type I migration timescale at the time of migration (e.g., Kokubo & Ida 1998; Ogihara & Ida 2009). In this case, the inner planet starts to migrate before the outer planet does, resulting in an expansion of the orbital separation ($\Delta > 10r_H$). On the other hand, as planets grow, the surrounding planetesimals stirred by the planets are fragmented by mutual collisions. The resultant fragments effectively accrete onto planets (Kobayashi et al. 2010, 2011); t_g depends on the initial planetesimal mass and radial gas density profile, and t_g might be shorter than t_a in some cases (Kobayashi et al. 2010, 2012) when migration begins. If $t_g \lesssim t_a$, the two planets can start their migration almost simultaneously, in which case the orbital separation ($\Delta \simeq 10r_H$) is maintained during migration. Detailed calculations that include accretion, fragmentation, and migration are needed to clarify this behavior.

6.1.2. Systems in Closely Spaced Resonances: Kepler-11 and Kepler-60

Below we discuss some individual systems. First, in this subsection the systems in closely spaced resonances (e.g., 4:3 and 5:4) are considered. As shown in Figure 11, the differences in $t_{a,\text{crit}}$ between adjacent pairs are small; for instance, the $t_{a,\text{crit}}$ difference between the 4:3 and 5:4 resonances is only a factor of two. This means that the migration speeds for systems in closer resonances can be

constrained well.

The Kepler-11 system, in which six planets have been confirmed, has a possible pair of planets in a 5:4 mean motion resonance (planets b and c). The critical migration timescales for the 4:3 and 5:4 resonances are $3 \times 10^3 T_K$ and $1.5 \times 10^3 T_K$, respectively. Thus, if these planets are formed well separated from each other ($\Delta > 10r_H$) and then undergo convergent migration, the migration timescale would be a few thousand times T_K . This migration speed is slightly higher than that of type I migration ($C_{1f_g} \gtrsim 1$). Because the other planets in the Kepler-11 system are not considered in resonances, it may not be natural to suppose that the planets undergo significant migration. Therefore, it seems likely that they are formed *in situ* and exhibit slight inward migration, which leads to capture into the 5:4 resonance. In addition, the required high type I migration speed is inconsistent with the typical migration speed which is predicted by the population synthesis model (Ida & Lin 2008), which would also support the *in situ* formation. The orbital separation is slightly smaller than the typical orbital separation after oligarchic growth at 1 AU ($\simeq 10r_H$); however, it has been shown that planets can be formed with smaller orbital separations near the central star ($\simeq 7r_H$) (Ogihara & Ida 2009). It is also possible that the planets formed *in situ* and planet b exhibited outward migration due to the tidal torque from the central star, resulting in capture into the resonance. Note that the difficulty of *in situ* accretion was pointed out in an investigation of the accretion and evolution of a hydrogen-rich atmosphere for Kepler-11 (Ikoma & Hori 2012). Another possibility is that the planets are formed in distant orbits and migrate inward as a resonant convoy, in which the planets can pass through 2:1 resonances as they are pushed inward by the outer bodies in the resonances (Ogihara & Ida 2009). However, in such a case, it is likely that other planets are also in resonances in the final state.

The Kepler-60 system consists of three planets: the inner pair (b and c) has 5:4 commensurability, and the outer pair (c and d) seems to be in a 4:3 resonance. If we assume that these planets formed well separated and then migrated inward, the differential migration timescale would be approximately $5 \times 10^3 - 1 \times 10^4 T_K$. Using Equation (21), we find that the efficiency of type I migration multiplied by the scaling factor for the gas surface density is $C_{1f_g} \simeq 1$. This means that if the gas surface density is similar to that of the minimum-mass solar nebula, the migration speed would be that predicted by the linear theory of type I migration (Tanaka et al. 2002). We also do not exclude the possibility of an *in situ* formation model for this system.

6.1.3. Systems with Small Separations: HD 200964, HR 8799, HD 45364, and Gliese 876

Next, we discuss resonant systems with small orbital separations ($\Delta \lesssim 2\sqrt{3}r_H$), which can be Hill unstable. In the HD 200964 system, two Jovian-mass planets lie in a 4:3 mean motion resonance (e.g., Johnson et al. 2011; Wittenmyer et al. 2012), and their orbital separation is $\simeq 1.5r_H$. If we assume that these planets are stable despite their small separation, the differential migration timescale for passing through the 3:2 resonance would be extremely short ($\simeq 60T_K$). This migration speed is al-

most impossible to achieve because a large amount of angular momentum should be delivered to the disk. Thus, it is not easy to provide a formation model that produces the orbital properties of the HD 200964 system. In fact, Rein et al. (2012) have also claimed that no formation scenarios are successful in reproducing 4:3 resonant planets similar to those in the HD 200964 system. Because the pair of planets around HD 200964 have almost crossing orbits, they might be in temporary resonance following orbital instability.

The HR 8799 system has inner and outer debris disks (Reidemeister et al. 2009) and four planets that were discovered by direct imaging (Marois et al. 2008, 2010). The masses have not been well constrained; the planets have masses between a few and 13 Jupiter masses (e.g., Marley et al. 2012). Because the orbital separations of the second innermost pair (planets d and c) and the outermost pair (planets c and b) are small ($\simeq 3r_{\text{H}}$), it is plausible that the two pairs of planets are in 2:1 mean motion resonances, which can stabilize the system over the estimated age of the star (Reidemeister et al. 2009; Fabrycky & Murray-Clay 2010). In this case, our model gives a lower limit on the migration timescale of $40T_{\text{K}}$. This value is quite small, so it may not provide a useful constraint. In addition to this lower limit, the time of passage of the Hill unstable region should be shorter than the orbital unstable time for a system with small orbital separation ($\Delta \lesssim 2\sqrt{3} r_{\text{H}}$). According to Fabrycky & Murray-Clay (2010), the crossing time, which is the timescale of the initiation of orbital instability, is $\simeq 3 \times 10^5 \text{ yr} = 3 \times 10^3 T_{\text{K}}$; therefore, the actual migration timescale would be between $40 T_{\text{K}}$ and $3 \times 10^3 T_{\text{K}}$. The type II migration expected for such massive planets cannot bring about the short migration timescale. Reidemeister et al. (2009) pointed out that if the masses of the planets are small, the system can be Hill stable.

Gliese 876, an M-dwarf star with a mass of $0.33M_{\odot}$, harbors four planets: planets c and b have comparable masses, and planets d and e are relatively small, with masses of $\sim 10M_{\oplus}$. Planets c–b and b–e are in or close to the 2:1 resonance. The orbital separations for the inner pair (c–b) and the outer pair (b–e) are $3.2r_{\text{H}}$ and $3.5r_{\text{H}}$, respectively. These planets are believed to be in the 2:1 resonance to stabilize their orbits at such a small orbital separation (e.g., Marcy et al. 2001). The lower limits to the differential migration timescales are $40T_{\text{K}}$ for the inner pair and $400T_{\text{K}}$ for the outer pair, which is consistent with the migration timescale obtained from a hydrodynamical simulation of this system by Kley et al. (2004).

Finally in this subsection, we add some comments on planets with small separations that are still Hill stable. The HD 45364 system consists of two planets with masses comparable to those of Saturn and Jupiter (Correia et al. 2009), which seem to be in a 3:2 mean motion resonance with a separation of $3.9r_{\text{H}}$. This system should have undergone rapid migration to pass through the 2:1 resonance. The critical migration timescale for capture into the 2:1 resonance is given by $t_{a,\text{crit}} \simeq 10^3 T_{\text{K}}$; thus, the differential migration timescale should be at least shorter than $10^3 T_{\text{K}}$. Rein et al. (2010) also examined this system both numerically and analytically, and proposed that a

relative migration timescale shorter than $800T_{\text{K}}$ is needed to pass through the 2:1 resonance, which is consistent with our results. Our model also provides a lower limit of $200T_{\text{K}}$ on the migration timescale. The planets in this system would have undergone type III migration.

6.2. Other Systems

Here we apply our results to resonant systems in the solar system. One good example is the Galilean satellites around Jupiter, where Io–Europa and Europa–Ganymede are in the 2:1 mean motion resonance. Replacing the stellar mass (M_{\star}) with the Jupiter mass, our model gives a lower limit of $1 \times 10^4 T_{\text{K}}$ on the differential migration speed. This constraint is consistent with the result of N -body work on the formation of the Galilean satellites (Equation [32] in Ogihara & Ida 2012).

Some trans-Neptunian objects are in mean motion resonance with Neptune. The population of objects in the 3:2 resonance is much higher than that in the 2:1 resonance. The objects were captured into the mean motion resonances during outward migration of Neptune. Simulations by Ida et al. (2000) showed that the tendency could be explained by the migration speed of Neptune. We apply our formula for the inward migration of the outer objects to resonant capture by an outwardly migrating Neptune. The obtained migration timescale of 3–10 Myr is plausible for the high population of the 3:2 resonance, which is roughly consistent with Ida et al. (2000). Furthermore, this estimated migration timescale is also consistent with that obtained by Murray-Clay & Chiang (2005) of 1–10 Myr, which is derived from studying the proportion of TNOs in the leading and trailing islands of the 2:1 resonance. Neptune’s outward migration, which is caused by interaction with the surrounding planetesimals, and other planets may not be as smooth as we assume (Levison et al. 2008). The application of our model to these objects should be done carefully.

We can further discuss other planet formation models, which assume the establishment of mean motion resonances. In the Grand Tack model (Walsh et al. 2011), Saturn migrates faster than Jupiter, which results in capture into a 3:2 mean motion resonance with Jupiter. For capture into the 3:2 resonance, the differential migration timescale between the two planets should be 100–500 T_{K} , which is smaller than the typical type I or II migration timescales. Walsh et al. (2011) considered high-speed type III migration, which is necessary to realize the Grand Tack scenario.

7. CONCLUSION

We investigated capture into first-order mean motion resonances in a system of two bodies undergoing damping of the eccentricity and semimajor axis using N -body integrations. In some of our calculations, we considered the case in which the mass of one body is negligible. In addition, we also studied systems with equal masses. In fact, orbital calculations were performed with a wide range of parameters; we found that the critical migration timescale can be described using the mass ratio between the larger body and the central object, and depends weakly on the e -damping timescale and initial eccentricity. The empirical formula is given by Equation (4), where the critical migration timescale for equal-mass bodies is about an order of magnitude shorter than

that for systems with a massless particle. We also confirmed the power-law dependence of the mass with index $-4/3$. This dependence is also supported by analytical arguments that compare the resonant libration timescale and the migration timescale. Additional simulations of closely spaced resonances were run, and empirical fits to the results were derived. All the fitting formulae from our calculations are shown in Figure 10 and Table 2.

The empirical formula we derived can constrain the relative migration speed in systems of two bodies undergoing convergent migration toward capture into mean motion resonances. This means that our model can be useful for understanding the origins of exoplanet systems in resonances. For systems in closely spaced mean motion resonances (e.g., Kepler-11, Kepler-60), the migration timescale can be well constrained. It is also possible that the planets formed *in situ*. The systems in which the orbital separation is smaller than $2\sqrt{3}r_H$ (e.g., HR 8799, Gliese 876) are believed to become stable owing to resonant effects. Lower limits to the relative migration timescale were placed on several systems in 2:1 resonances. The origin of the HD 200964 system, which is in 4:3 resonance, remains unclear. Our model also provides constraints on the migration timescale of systems other than exoplanets (e.g., the Grand Tack model of the solar system). Furthermore, when the number of discov-

ered exoplanets in resonances increases sufficiently in the future, the typical type I and II migration timescales can be obtained using our results; future observations will allow us to tackle this issue. Note that if the eccentricity at a resonant encounter is large, the capture into resonance becomes probabilistic. In this case, our model can provide only a necessary condition.

In this work, we considered first-order mean motion resonances, which are certainly important for planets both inside and outside the solar system. In addition, higher-order mean motion resonances (e.g., 3:1 and 5:2) can also be important for specific systems (e.g., Michtchenko & Ferraz-Mello 2001; Steffen 2013); therefore, it would be worth examining the conditions for capture into these resonances in future work.

ACKNOWLEDGMENT

We thank to an anonymous referee for detailed helpful comments. We also thank S. Inutsuka for helpful discussions. The numerical computations were conducted in part on the general-purpose PC farm at the Center for Computational Astrophysics, CfCA, of National Astronomical Observatory of Japan. This work was supported by a Grant-in-Aid for JSPS Fellows (23004841). HK gratefully acknowledges the support of a Grant-in-Aid from MEXT (23103005).

REFERENCES

- Barnes, R., & Greenberg, R. 2005, *ApJ*, 647, L163
 Baruteau, C., & Papaloizou, J. C. B. 2013, *ApJ*, submitted
 Cochran, W. D. et al. (2011) *ApJS*, 197, 7
 Correia, A. C. M., Udry, S., Mayor, M., Benz, W., Bertaux, J.-L., Bouchy, F., Laskar, J., Lovis, C., Mordasini, C., Pepe, F., & Queloz, D. 2009, *A&A*, 496, 521
 Fabrycky, D. C., & Murray-Clay, R. A. 2010, *ApJ*, 710, 1408
 Friedland, L. 2001, *ApJ*, 547, L45
 Gladman, B. 1993, *Icarus*, 106, 247
 Goldreich, P. 1965, *MNRAS*, 130, 159
 Hayashi, C. 1981, *Prog. Theor. Phys. Suppl.*, 70, 35
 Henrard, J. 1982, *Celest. Mech.*, 27, 3
 Ida, S. Bryden, G., Lin, D. N. C., & Tanaka, H. 2000, *ApJ*, 534, 428
 Ida, S. & Lin, D. N. C. 2008, *ApJ*, 673, 484
 Ikoma, M., & Hori, Y. 2012, *ApJ*, 753, 66
 Johnson, J. A., Payne, M., Howard, A. W., Clubb, K. I., Ford, E. B., Bowler, B. P., Henry, G. W., Fischer, D. A., Marcy, G. W., Brewer, J. M., Schwab, C., Reffert, S., & Lowe, T. B. 2011, *AJ*, 141, 16
 Kley, W., Peitz, J., & Bryden, G. 2004, *A&A*, 414, 735
 Kobayashi, H., Ormel, C. W., & Ida, S. 2012, *ApJ*, 756, 70
 Kobayashi, H., Tanaka, H., & Krivov, A. V. 2011, *ApJ*, 738, 35
 Kobayashi, H., Tanaka, H., Krivov, A. V., & Inaba, S. 2010, *Icarus*, 209, 836
 Kokubo, E. & Ida, S. 1998, *Icarus*, 131, 171
 Lissauer, J. J. et al. 2011, *ApJS*, 197, 8
 Levison, H. F., Morbidelli, A., VanLaerhove, C., Gomes, R., & Tsiganis, K. 2008, *Icarus*, 196, 258
 Makino, J., & Aarseth, S. J. 1992, *Publ. Astron. Soc. Jpn.*, 44, 141
 Marley, M. S., Saumon, D., Cushing, M., Ackerman, A. S., Fortney, J. J., & Freedman, R. 2012, *ApJ*, 754, 135
 Marois, C., Macintosh, B., Barman, T., Zuckerman, B., Song, I., Patience, J., Lafrenière, D., & Doyon, R. 2008, *Science*, 322, 1348
 Marois, C., Zuckerman, B., Konopacky, Q. M., Macintosh, B., & Barman, T. 2010, *Nature*, 468, 1080
 McNeil, D., Duncan, M. J., & Levison, H. F. 2005, *AJ*, 130, 2884
 Marcy, G. W., Butler, R. P., Fischer, D., Vogt, S. S., Lissauer, J. J., Rivera, E. J. 2001, *ApJ*, 556, 296
 Mayor, M., Udry, S., Lovis, C., Pepe, F., Queloz, D., Benz, W., Bertaux, J.-L., Bouchy, F., Mordasini, C., & Segransan, D. 2009, *A&A*, 493, 636
 Michtchenko, T. A., & Ferraz-Mello, S. 2001, *Icarus*, 149, 357
 Murray, C. D., & Dermott, S. F. 1999, *Solar System Dynamics* (Cambridge: Cambridge Univ. Press)
 Murray-Clay, R. A., & Chiang, E. I. 2005, *ApJ*, 619, 623
 Mustill, A. J., & Wyatt, M. C. 2011, *MNRAS*, 413, 554
 Nelson, R. P., & Papaloizou, J. C. B. 2002, *MNRAS*, 339, 993
 Ogihara, M., & Ida, S. 2009, *ApJ*, 699, 824
 Ogihara, M., & Ida, S. 2012, *ApJ*, 753, 60
 Ogihara, M., Duncan, M. J., & Ida, S. 2010, *ApJ*, 721, 1184
 Paardekooper, S.-J., Baruteau, C., & Kley, W. 2011, *MNRAS*, 410, 293
 Papaloizou, J. C. B., & Szuszkiewicz, E. 2005, *MNRAS*, 363, 153
 Quillen, A. C. 2006, *MNRAS*, 365, 1367
 Raymond, S. N., Barnes, R., Armitage, P. J., & Gorelick, N. 2008, *ApJ*, 687, L107
 Reidemeister, M., Krivov, A. V., Schmidt, T. O. B., et al. 2009, *A&A*, 503, 247
 Rein, H. 2012, *MNRAS*, 427, L21
 Rein, H., Papaloizou, J. C. B., & Kley, W. 2010, *A&A*, 510, A4
 Rein, H., Payne, M. J., Veras, D., & Ford, E. B. 2012, *MNRAS*, 426, 187
 Snellgrove, M. D., Papaloizou, J. C. B., & Nelson, R. P. 2001, *A&A*, 374, 1092
 Steffen, J. H. 2013, *MNRAS*, submitted
 Steffen, J. H. et al. 2013, *MNRAS*, 428, 1077
 Szuszkiewicz, E., & Podlowska-Gaca, E. 2012, *Orig. of Life and Evol. of the Biosph.*, 42, 113
 Origins of Life and Evolution of the Biosphere, 42, 113
 Tanaka, H., Takeuchi, T., & Ward, W. R. 2002, *ApJ*, 565, 1257
 Terquem, C., & Papaloizou, J. C. B. 2007, *ApJ*, 654, 1110
 Veras, D., & Mustill, A. J. 2013, *MNRAS*, in press.
 Walsh, K. J., Morbidelli, A., Raymond, S. N., O'Brien, D. P., Mandell, A. M. 2011, *Nature*, 475, 206
 Weidenschilling, S. J., & Davis, D. R. 1985, *Icarus*, 62, 16
 Wisdom, J. 1980, *AJ*, 85, 8
 Wittenmyer, R. A., Horner, J., & Tinney, C. G. 2012, *ApJ*, 761, 165
 Wyatt, M. C. 2003 *ApJ*, 598, 1321
 Zhou, J.-L., & Lin, D. N. C. 2007, *ApJ*, 666, 447

TABLE 3
SYSTEMS IN OR NEAR FIRST-ORDER MEAN MOTION RESONANCES

Star	$M_*(M_\odot)$	Planet	$M(M_\oplus)$	a (AU)	MMR [pair]	Period ratio
Gliese 876	0.334	d	6.68	0.0208		
		c	227	0.130	2:1 [b]	2.03
		b	723	0.208	2:1 [e]	2.03
		e	14.6	0.334		
HD 37124	0.83	b	215	0.534		
		c	207	1.71	2:1 [d]	2.10
		d	221	2.81		
HD 73526	1.08	b	922	0.66	2:1 [c]	2.00
		c	795	1.05		
HD 82943	1.18	c	639	0.746	2:1 [b]	2.01
		b	556	1.19		
HD 128311	0.84	b	693	1.10	2:1 [c]	2.05
		c	1020	1.76		
HR 8799	1.56	e	2861	15		
		d	3179	27	2:1 [c]	2.00
		c	3179	43	2:1 [b]	1.99
		b	2225	68		
Kepler-9	1	d	6.99	0.0273		
		b	80.1	0.14	2:1 [c]	2.02
		c	54.4	0.225		
Kepler-18	0.972	b	6.90	0.0447		
		c	17.2	0.0752	2:1 [d]	1.94
		d	16.5	0.117		
Kepler-48	0.89	b	4.79		2:1 [c]	2.02
		c	10.6			
Kepler-51	1.00	b	55.9		2:1 [c]	1.89
		c	36.2			
Kepler-52	0.54	b	4.61		2:1 [c]	2.08
		c	3.51			
Kepler-53	0.98	b	8.90		2:1 [c]	2.07
		c	10.8			
Kepler-56	1.37	b	16.0		2:1 [c]	2.04
		c	69.7			
Kepler-57	0.83	b	5.03		2:1 [c]	2.03
		c	2.47			
mu Ara	1.08	c	10.6	0.0909		
		d	166	0.921	2:1 [b]	2.07
		b	533	1.5		
		e	577	5.235		
24 Sex	1.54	b	633	1.33	2:1 [c]	1.95
		c	273	2.08		
HD 45364	0.82	b	59.5	0.681	3:2 [c]	1.51
		c	209	0.897		
Kepler-49	0.55	b	7.86		3:2 [c]	1.51
		c	6.88			
Kepler-54	0.51	b	4.61		3:2 [c]	1.51
		c	1.53			
Kepler-55	0.62	b	6.23		3:2 [c]	1.51
		c	5.12			
Kepler-58	0.95	b	8.22		3:2 [c]	1.52
		c	8.71			
Kepler-59	1.04	b	1.22		3:2 [c]	1.51
		c	4.08			
HD 200964	1.44	b	588	1.60	4:3 [c]	1.34
		c	286	1.95		
Kepler-60	1.11	b	5.46		5:4 [c]	1.25
		c	6.44		4:3 [d]	1.33
		d	6.88			
Kepler-11	0.961	b	4.30	0.091	5:4 [c]	1.26
		c	13.5	0.106		
		d	6.10	0.159		
		e	8.40	0.194		
		f	2.30	0.25		
		g	302	0.462		
Kepler-50	1.24	b	5.07	0.077	6:5 [c]	1.20
		c	8.28	0.087		

NOTE. — Values are taken from the Open Exoplanet Catalogue. Shown (left to right) are the Star, the stellar mass, the identifier of the planet, the planet mass, the semimajor axis, the commensurability of the resonant pair, and the period ratio of the resonant pair.